Soft Matter

Accepted Manuscript

ROYAL SOCIETY OF CHEMISTRY

www.rsc.org/softmatter

Journal Name

RSCPublishing

ARTICLE

Directional supracolloidal self-assembly via dynamic covalent bonds and metal coordination

Cite this: DOI: 10.1039/xoxxoooooox

Na Xu, Jie Han, Zhengguang Zhu, Bo Song, Xinhua Lu and Yuanli Cai*

Received ooth January 2012,
Accepted ooth January 2012

DOI: 10.1039/xoxxoooooox

www.rsc.org/

An emerging strategy towards the sophistication of supramolecular nanomaterials is the use of supracolloidal self-assembly, in which the micelles or colloids are used as building blocks. Binding directionality can produce the nanostructures with attractive properties. Herein, we present a new directional supracolloidal self-assembly by virtue of dynamic covalent bonds and metal coordination in water. Conjugation of a ligand precursor to a water-soluble block copolymer through dynamic covalent bonds leads to the dehydration and micellization of the functionalized polymer. Reversible reaction facilitates the permeation of metal ions into the core-shell interfaces. Conversely, metal-coordination promotes reaction over the interfaces. Cu(II)-coordination occurs overwhelmingly inside each isolated micelle. However, Zn(II)-coordination induced a directional self-assembly whose nanostructures evolve stepwise from nanorods, nanowires, necklaces, and finally to supracolloidal networks scaling-up to several tens of micrometres. Post reactions of simultaneous dynamic covalent bond conversion and Zn(II)-coordination over the core-shell interfaces endow these supracolloidal networks with a huge specific surface area for hydrophobic dative metal centres accessible to substrates in water. Water-soluble shells play important roles in directional supracolloidal assembly and in the stabilization of nanostructures. Thus the directional self-assembly provides a versatile platform to produce metallo-hybridized nanomaterials for enzyme-inspired aqueous catalysts.

Introduction

Self-assembly of colloid particles into sophisticated directional nanostructures has attracted considerable attention over the last ten years. This can offer mechanical, electronic and magnetic properties that are essential in a range of important applications, e.g., energy storage,[1] therapy[2] and electronics.[3] Supracolloidal assemblies were enabled by recent breakthroughs in the colloid synthesis.[4-10] Incorporating directionality in shape[11] and surface functionality[12] introduces a bonding directionality, and extends nanostructures as complex as those seen in molecular crystals.[9] Recent achievements unveiled fascinating potentials to translate this idea to colloid building blocks.[13-16] Majority of the recent supracolloidal self-assembly that were exploited by Müller and other groups[4-10] was achieved by virtue of selective solvophobic interactions. Obviously, exploring of a strategy to high binding directionality is indispensable to achieve the sophistication in supracolloidal nanostructures.

Metal-coordination provides a perfect flexibility in rationale design of nanomaterials. The coordination of polymeric motifs has been evolved into a powerful tool for fabrication of hybrid functionalized materials.[17] It was employed for self-assembly of block copolymers into metallogel and other nanostructures.[18, 19] Recent results illustrated the effectiveness in the production of antimicrobial[20] and self-healing[21] materials, stiffened films,[22] polypeptide nanostructures,[23] helical metal-polymers[24] and even chirality-tuned particles.[25] Gohy and co-workers[26-28] described the elegant examples of metallogel via coordination of micelle-shell chain-ends. Weck and co-workers[29] exploited the patchy particle assembly *via* Pd-coordination in organic solution.

Herein, we report a general and versatile strategy toward a directional supracolloidal self-assembly *via* dynamic covalent bonds and coordination with abundant transition metal ions in water. To this end, poly(2-aminoethylmethacrylamide hydrochloride)-*block*-poly(2-hydroxypropylmethacrylamide) (PAEMA-*b*-PHPMA) was obtained via reversible addition-fragmentation chain transfer (RAFT) polymerisation under visible light irradiation at 25°C.[30, 31] The hydrophobic terdendate ligand motifs can be achieved by reaction of their NH_2 groups with pyridine-2,6-dicarboxaldehyde (PDCA) via an imine conversion (Fig. 1). These ligand motifs have high coordination constants with the abundant first-row transition metal ions, such as copper ions and zinc ions.[32, 33] The environment of dative metal centres can be tuned by assembling into hydrophobic domains in water,[34-36] thus are potential in the enzyme-inspired aqueous catalysts.[34-37] Moreover, reversible imine bonds facilitate permeation of metal ions into hydrophobic domains because the residual NH_2-motifs favoured the enrichment of metal ions onto these interfaces for dative-bonding association. Accordingly, the reversible imine

conversion, dehydration and micellization, and self-assembly of these micelles via coordination with copper and zinc ions were studied by ^{1}H NMR, UV-vis/FTIR spectroscopy, dynamic light scattering, atomic force microscopy and transmission electron microscopy.

Experimental section

Materials

The details for the synthesis of water-soluble block copolymers are described in Electronic Supplementary Information (ESI) and Figs. S1-2. PDCA was purchased from TCI; zinc acetate and copper acetate were from Aladdin; deuterium oxide (D_2O) from J&K; these agents were used as received. Triethylamine (TEA) was refluxed over CaH_2. Deionized water with R > 18.2 MΩ/cm was obtained from an AQUELX 5 Millipore.

Dynamic imine conversion and micellization in water

Typically, $PAEMA_{57}$-*b*-$PHPMA_{56}$ (30 mg, 1.7 μmol, [AEMA]= 39 mM) was dissolved in D_2O (2.78 g); PDCA (8.1 mg, 60 μmol) was dissolved in D_2O (20.0 g). Stock solutions of PDCA (1.67 g) and copolymer (0.278 g) were mixed in a 10-mL vial. TEA (1.2 M in D_2O) was added drop-wise to a predetermined solution pH. Reaction was equilibrated at 25°C overnight, and then moved to a NMR tube for ^{1}H NMR. The micellization was studied as the follows. $PAEMA_{57}$-*b*-$PHPMA_{56}$ (0.50 g, 6.0 mg/mL in water, [AEMA]=19 mM) and PDCA (3.0 g, 1.67 mM in water) were mixed in a 10-mL vial. TEA (60 mM in water) was added to adjust to pH 9.5. The reaction and phase transition were monitored using UV spectroscopy and DLS at 25°C. These particles were measured by DLS, AFM and TEM after equilibration at ambient temperature for 2 days.

Supracolloidal self-assembly *via* metal coordination in water

Typically, zinc acetate was added in the solution of equilibrated micelles to $[Zn(II)]_0/[ligand]_0$=0.3. Coordination was monitored using ^{1}H NMR and UV-vis spectroscopy; the aggregation was monitored by DLS. The nanostructures were visualized by DLS, AFM and TEM after equilibration at 25°C for 2 days.

Simultaneous imine-bond conversion and metal coordination

$PAEMA_{57}$-*b*-$PHPMA_{56}$, PDCA and zinc acetate were mixed in water to a $[AEMA]_0$:$[PDCA]_0$:$[Zn(II)]_0$=2:1:0.3 in a 10-mL vial. The reaction was monitored by ^{1}H NMR and UV spectroscopy immediately after adjusting to pH 9.5. The phase transition was monitored using DLS. Their structures were visualized by DLS and AFM after equilibration at room temperature for 2 days.

^{1}H NMR spectroscopy

^{1}H NMR spectra were recorded on an INOVA 400MHz NMR instrument under scanning for 32 times at 25°C.

UV-visible spectroscopy

Typically, $PAEMA_{57}$-*b*-$PHPMA_{56}$ (0.50 g, 6.0 mg/mL in water, [AEMA]=19 mM) and PDCA (3.0 g, 1.67 mM in water) were mixed in a 10-mL vial. The solution was diluted with water to a 75 mg/L of polymer, and then moved to a quartz cuvette. After adjusted to pH 9.5 using TEA (60 mM in water), UV-vis spectra were recorded on a Shimadzu UV-3600 UV-visible spectrometer at predetermined time points at 25°C.

FTIR spectroscopy

FTIR spectroscopy was conducted on a Nicolet 6700 FTIR spectrometer. Reaction was equilibrated at ambient temperature for 2 days. The solution was dropped on calcium fluoride tablet. Sample was dried under vacuum at ambient temperature.

Dynamic light scattering (DLS)

DLS was performed on a Brookhaven BI-200SM setup that was equipped with a 22-mW He-Ne laser (λ=633 nm), a BI-200SM goniometer and a BI-TurboCorr digital correlator at a scattering angle of 90°. The solution was controlled at 25±0.02°C by a BI-TCD controller. Laser intensity was attenuated down to 50% of the original. The intensity-average hydrodynamic diameters (D_h) and dispersity (μ_2/Γ^2) were assessed by cumulants analysis in CONTIN routine. Data were averaged over three times.

Atomic force microscopy (AFM)

AFM imaging was performed on a Bruker Multimode 8 microscope operated in a peak force quantitative nanomechanical scan mode using a SCANASYST-AIR probe (spring constants: 0.4 N/m, resonance frequency: 70 kHz, tip radius: 2 nm). Silicon wafer was immersed in the mixture of 98% H_2SO_4 and 35% H_2O_2 (7:3, v/v) for 2 h, and thoroughly rinsed with water. As-cast solution on silicon wafer was lyophilized in a Labconco Freezone 2.5L freeze-drier.

Transmission electron microscopy (TEM)

TEM was conducted on Hitachi HT7700 transmission electron microscope at an accelerating voltage of 200 kV. The as-cast solution on carbon film-coated copper grid was lyophilized in a Labconco Freezone 2.5L freeze-drier.

Results and discussion

PAEMA-*b*-PHPMA was synthesized by the sequential aqueous RAFT polymerisation under visible light irradiation at 25°C[38, 39] (ESI, Figs. S1-2). The polymerisation proceeds rapidly and can start-up/suspend immediately after turning on/off visible light, so that degree of polymerisation (DP) can be controlled during chain extension.[31] $PAEMA_{57}$-*b*-$PHPMA_{56}$ and $PAEMA_{47}$-*b*-$PHPMA_{247}$ (polydispersity indices PDIs<1.10) were selected, in which PHPMA blocks are biocompatible and water-soluble,[40] and the ionic primary amine groups (NH_3^+) of PAEMA blocks can be converted into reactive NH_2 motifs upon adding TEA.[41] PDCA was selected as a ligand precursor, because their imine derivatives are perfect terdendate ligands (Fig. 1) for abundant first-row transition metal ions,[32] such as ferrous, cobalt, nickel, copper and zinc ions.[33] Hence, copper acetate and zinc acetate were used to mediate the directional supracolloidal assembly of PDCA-conjugated polymer micelles via dative bonds in water.

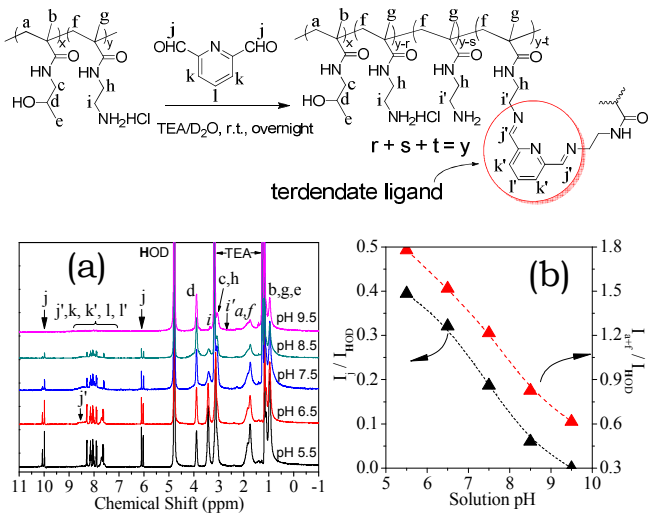

Fig. 1 (**a**) ^{1}H NMR spectra of the solutions of PAEMA$_{57}$-*b*-PHPMA$_{56}$ and PDCA at a [AEMA]$_0$/[PDCA]$_0$=2 (1.50 g/L of polymer) in D_2O at predetermined solution pH; (**b**) the variation of the integral ratios of signals *j* (*black*, C**H**O in PDCA) and *a+f* (C**H**$_2$C(CH$_3$) in backbone of both units) to that of **H**OD impurities.

Dynamic imine conversion and micellization in water

As shown in Fig. 1a, the signal *d* (C**H**OH in HPMA units) was discernible in D_2O over pH 5.5~9.5. This signal was used as an internal standard to evaluate imine conversion. The signals over δ=7.0~9.0 ppm (3H in PDCA pyridine rings) decreased with alkalization. Based on the acid-base titration results (Fig S3a), NH_3^+ motifs started to convert into NH_2 forms upon alkalization above pH 4.7 wherein copolymer maintained soluble in water at pH 9.5 (Fig. S3b). Alkalization from pH 7.1 led to deionization of PDCA into uncharged pyridine (Fig. S4). Hence, attenuation of signals over 7.0~9.0 ppm indicated the conjugation of PDCA to polymer chains. Moreover, a broadened C**H**=N signal *j'* at 8.7 ppm was detectable over pH 6.5~8.5, suggesting formation of imine bonds.[42, 43] It was also confirmed by the equilibration of small imine-derivatives at a 68% conversion (Fig. S5). The consumption of PDCA was revealed by a decrease in PDCA-aldehyde carbonyl FTIR peak ($\nu_{C=O}$)[32] at 1717 cm^{-1} (Fig. S6).

Furthermore, the signals *a*, *f* (C**H**$_2$ in backbone of both units) decreased with the solution pH, suggesting that PAEMA blocks have been dehydrated. C**H**$_2$NH$_2$HCl signal *i* (ionized AEMA units) attenuated after conversion into reactive NH_2 motifs, in which the signal should be up-field shifted to 2.7 ppm (*signal i'*, C**H**$_2$NH$_2$, Fig. S3b). The signal was undetected over pH 5.5~9.5, suggesting a dehydration of PDCA-conjugated units. Moreover, the integration of backbone signals *a*, *f* decreased with PDCA-consumption (Fig. 1b). These results demonstrate that PDCA-functionalized PAEMA-blocks have been dehydrated.

This reversible reaction was monitored by UV spectroscopy after adjusted to pH 9.5. As shown in Fig. 2a, a peak at λ_{max}= 275 nm red-shifted and the absorbance increased rapidly with reaction time. These variations were used to evaluate reaction kinetics. As shown in Fig. 2b, λ_{max} and absorbance levelled off shortly in 6 min, suggesting rapid equilibration of the reaction, which was akin to the rapid equilibration in the formation of amphiphilic imine-bonded compounds in water.[43] These results indicate that the dehydration of imine units and phase transition can promote this reversible reaction.

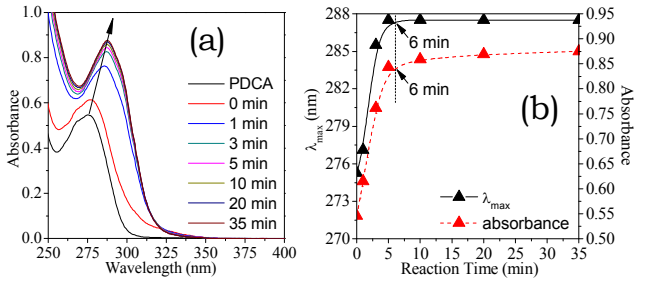

Fig. 2 (**a**) UV spectrum evolution on the conjugation of PAEMA$_{57}$-*b*-PHPMA$_{56}$ with PDCA ([AEMA]$_0$/[PDCA]$_0$=2, 75 mg/L of copolymer in water at pH 9.5); (**b**) the variation of characteristic wavelength (λ_{max}, *black*) and the absorbance (*red*).

Reaction-induced phase transition was thus monitored using dynamic light scattering (DLS). Before reaction, the solution of PAEMA$_{57}$-*b*-PHPMA$_{56}$ block copolymer was transparent and had low light scattering intensity at a 1.1 kcps in water at pH 9.5. Moreover, ^{1}H NMR revealed that their proton signals were completely detectable. These results demonstrate that the block copolymer has been dissolved in water.

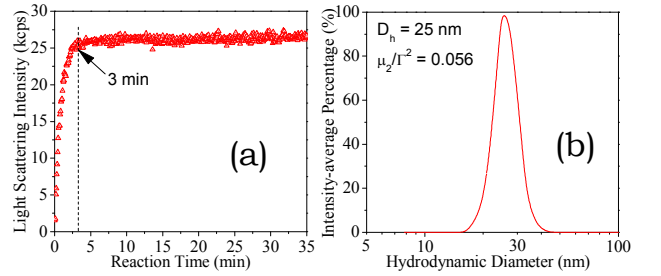

Fig. 3 (**a**) The evolution of light scattering intensity on conjugation of PAEMA$_{57}$-*b*-PHPMA$_{56}$ (0.75 g/L) with PDCA at [AEMA]$_0$/[PDCA]$_0$=2 in water at pH 9.5 and 25°C; (**b**) size distribution profile of the micelles formed after equilibration for 2 days.

Furthermore, in presence of PDCA at [AEMA]$_0$/[PDCA]$_0$=2 (Fig. 3a), the light scattering intensity increased immediately to 25.3 kcps after adjusted to pH 9.5 in 3 min. Hence, the PDCA-conjugation induced immediate phase transition. The solution maintained transparent after reaching a maximum intensity. DLS analysis revealed the formation of micelles at an intensity-average hydrodynamic diameter (D_h) of 25 nm and a dispersity (μ_2/Γ^2) of 0.056 (Fig. 3b) after equilibration for 2 days.

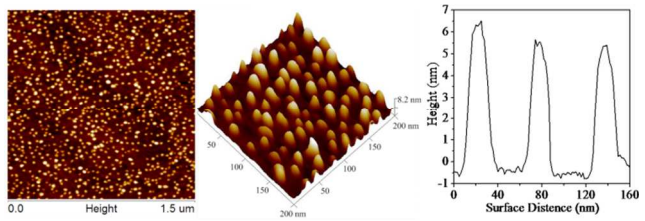

Fig. 4 AFM images of the micelles equilibrated under the conditions of Figure 3. The sample was prepared by lyophilisation of as-cast solution on silicon wafer.

AFM imaging (Fig. 4) revealed the soft spherical micelles with the cross sections of 25~30 nm in diameter and 6~7 nm in height. ^{1}H NMR studies demonstrated dehydration of PDCA-conjugated PAEMA blocks (Fig. 1a). These results demonstrate formation of micelles that are composed of PDCA-conjugated hydrophobic PAEMA-cores and water-soluble PHPMA-shells.

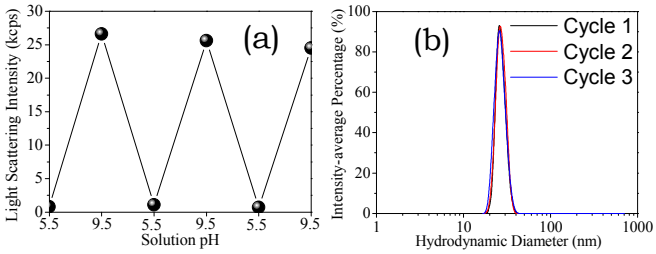

Fig. 5 (**a**) pH-responsive variation of the light scattering intensity of PAEMA$_{57}$-*b*-PHPMA$_{56}$ (0.75 g/L in water) in presence of PDCA at a [AEMA]$_0$/[PDCA]$_0$=2 upon cycling over pH 5.5-9.5, using TEA and 0.90 M HCl at 25°C; (**b**) size distribution profiles of the micelles formed at pH 9.5 in each cycle.

Furthermore, the reversibility in assembly-disassembly was elucidated by DLS upon cycling the solution pH over 5.5~9.5 for 3 times. As shown in Fig. 5a, the light scattering intensity varied periodically with the solution pH. More importantly, size distribution profile of the re-assembled micelles was perfectly consistent with those of the former (Fig. 5b), suggesting that the phase transition and the reassembled structures could be cycled reversibly in response to the solution pH.

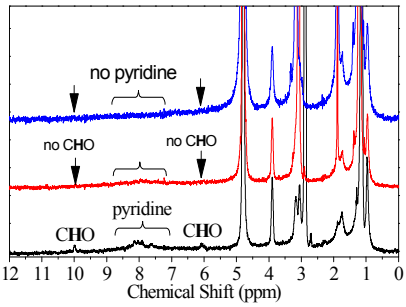

Fig. 6 ^{1}H NMR spectra of the micelles and those after coordinated with Zn(II) (*red*) and Cu(II) (*blue*) at [Mt(II)]$_0$/[ligand]$_0$=0.3 in D_2O at 25°C.

Supracolloidal self-assembly *via* metal-coordination in water

As illustrated in top scheme of Fig. 1, terdendate ligand motifs have been conjugated to PAEMA block after reversible reaction. It has been well known that the motifs have high coordination constants with the abundant first-row transition metal ions.[32, 33] Moreover, the chemical environment of the dative metal centres can be easily tuned by self-assembly into hydrophobic domains in water,[34-36] thus are promising as the metalloenzyme-inspired catalysts.[34-37] Inspired by such amazing potentials, Cu(II) and Zn(II) were used for directional supracolloidal self-assembly of as-obtained micelles *via* dative-bonding association in water.

As shown in Fig. 6, the weak C**H**O signals at 10.0, 6.1 ppm, and those in pyridine over 7.5~9.5 ppm were detected after the equilibration at room temperature for 2 days. After addition of metal ions, the C**H**O signal completely disappeared (*arrows*), suggesting that imine conversion has been promoted by metal-coordination.[41, 44] More importantly, signals in pyridine rings were detectable after Zn(II)-coordination but undetectable after Cu(II)-coordination, because their Cu(II)-complexes are more hydrophobic than Zn(II)-complexes (Fig. S7). Obviously, the residual hydrophilic NH_2 motifs favoured permeation of metal ions into the interfaces of hydrophobic micelle cores. Thus the post reactions of the simultaneous imine conversion and metal-coordination into partially hydrated Zn(II)-complex units led to directional self-assembling of these micelles into supracolloidal nanostructures and also stabilization of the nanostructures as to be discussed below.

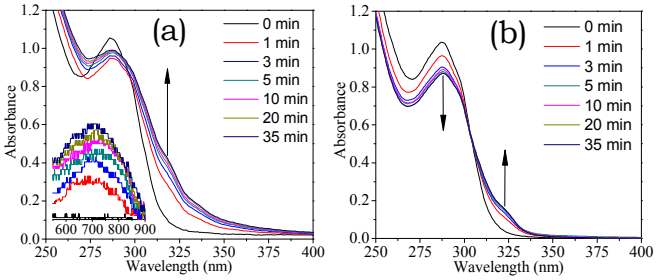

Fig. 7 The evolution of UV-vis spectra of PDCA-conjugated PAEMA$_{57}$-*b*-PHPMA$_{56}$ micelles upon coordination with (**a**) Cu(II) and (**b**) Zn(II) at [Mt(II)]$_0$/[ligand]$_0$=0.3.

Metal-coordination was followed by UV-vis spectroscopy immediately after addition of copper acetate or zinc acetate. As shown in Fig. 7, the absorbance at λ_{max}=286 nm decreased and a shoulder over λ=300~350 nm appeared immediately owing to coordination.[45] The formation of Cu(II)-complex units was also confirmed by a new peak over λ=550~900 nm (*insert* in Fig. 7a).[46] These results indicate that metal ions coordinated rapidly with hydrophobic imine motifs because of enhanced association of the residual hydrophilic NH_2 groups.

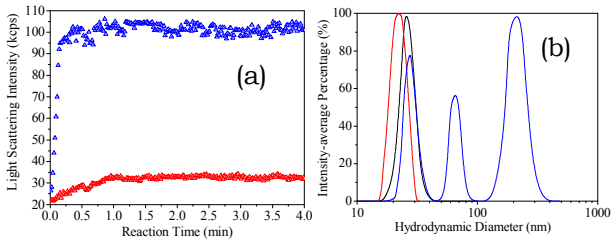

Fig. 8 (**a**) The evolution of light scattering intensity of PDCA-conjugated PAEMA$_{57}$-*b*-PHPMA$_{56}$ micelles (0.75 g/L of initial polymer in water) on adding Cu(II) (*red*) and Zn(II) (*blue*) at [Mt(II)]$_0$/[ligand]$_0$=0.3 at 25°C; (**b**) the size distribution profiles of the micelles (*black*) and those coordinated with Cu(II) (*red*) and Zn(II) (*blue*).

As shown in Fig. 8, these micelles have been shrunken from D_h=25 nm down to 22 nm after Cu(II)-coordination, leading to an increase in light scattering intensity from 22.3 to 33.0 kcps. These results indicate that copper ions have been coordinated overwhelmingly inside each isolated micelle. On the contrary, light scattering intensity increased dramatically to 105.0 kcps after Zn(II)-coordination. The overall sizes increased to a D_h= 120 nm and the dispersity broadened remarkably to 0.302 after Zn(II)-coordination wherein the aggregates were separated into

three size-regions, $D_{h,1}$=20~40 nm, $D_{h,2}$=50~90 nm (2~3×$D_{h,1}$), $D_{h,3}$=120~360 nm (4~12×$D_{h,1}$), which is a typical character in the step-growth polymerisation of nanoparticles.[47] These results demonstrate these coordination reactions have exerted entirely opposite controls over the reconstruction of the micelles.

Indeed, overwhelmingly compact spheres were formed after Cu(II)-coordination, as evidenced by an increase in height from 6~7 nm to 8~10 nm and a decrease in diameter from 25~30 nm to 20~25 nm (top images in Fig. 9). In contrast, Zn(II)-coordination led to formation of nanowires (bottom images in Fig. 9). Moreover, their undulating crests shown in 3D images and cross sections imply that dative association predominantly occurred over particle core-shell interfaces. The post reactions of simultaneous imine conversion and coordination endow huge specific surface area for hydrophobic dative metal centres that are accessible to the substrates in water medium.

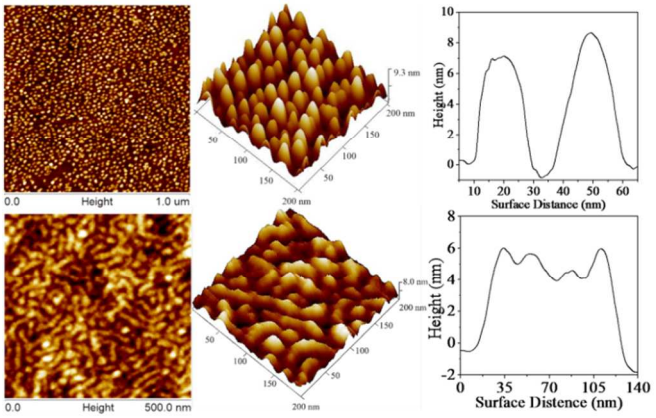

Fig. 9 AFM height, 3D images and the cross sections (*from left to right*) of the nanostructures, in which micelles were coordinated with Cu(II) (*top*) and Zn(II) (*bottom*) at a $[Mt(II)]_0/[ligand]_0$=0.3 in water.

The evolution of nanostructure was further elucidated by the stepwise increase of the feed ratio of zinc ions to ligand motifs ($[Zn(II)]_0/[ligand]_0$). AFM (left images in Fig. 10) revealed the stepwise directional growth of the nanostructures with increase of the ratio from 0.1 to 0.2, leading to the transformation from nanorods into necklaces. The nanostructures were transformed into nanowires upon increase to 0.3. Further increase to 0.5 led to transformation to supracolloidal networks.

TEM imaging (right images in Fig. 10) have evidenced the stepwise and directional features during the self-assembly of the micelles, in which the cores (central black dots) maintained after chain extension. These results further confirm that Zn(II)-coordination occurred predominantly surrounding the core-shell interfaces. Moreover, these metallo-hybridized supracolloidal networks have been up-scaled to several tens of micrometres. This unique hierarchical architecture endows huge specific surface area for hydrophobic dative metal centres essential for exploiting of metalloenzyme-inspired aqueous catalysts.[34-37]

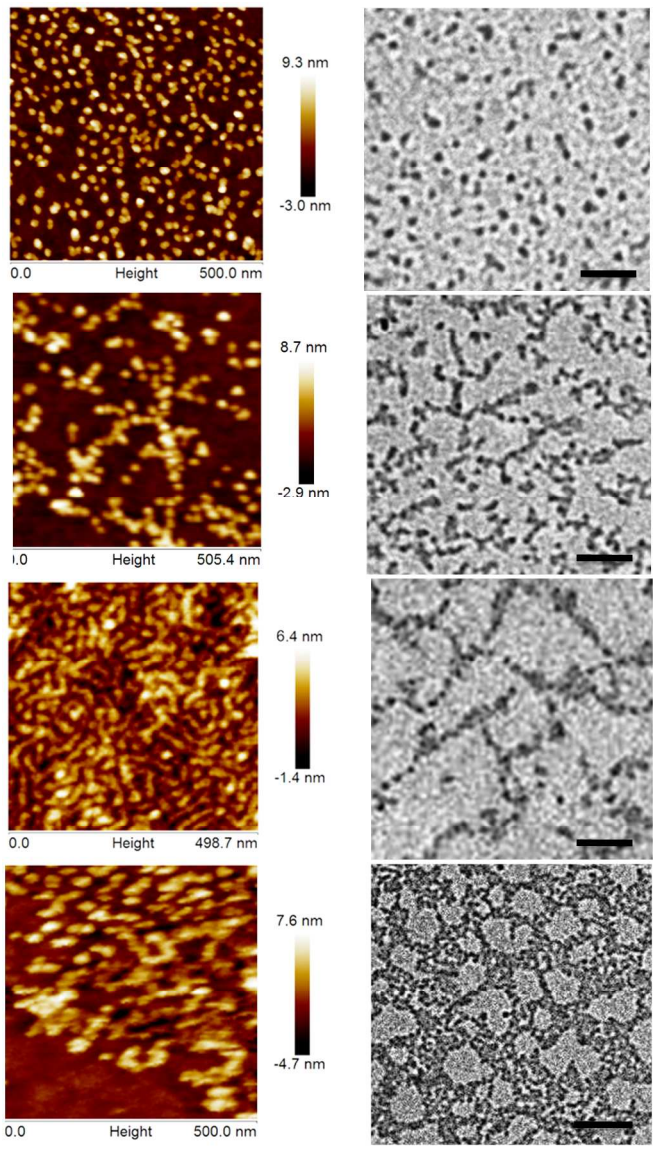

Fig. 10 AFM (*left*) and TEM (*right,* **bar**: 100 nm) images of the nanostructures regulated by coordination with Zn(II) upon varying $[Zn(II)]_0/[ligand]_0$ from 0.1, 0.2, 0.3 to 0.5 (*from top to bottom*). Herein, zinc acetate was added in the solution of micelles and allowed to equilibrate at ambient temperature for 2 days.

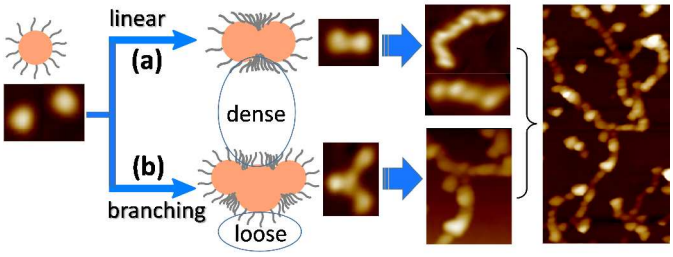

Fig. 11 Representative illustration for the directional self-assembly of micelles via Zn(II)-dative bonding association: (**a**) linear growth; (**b**) topological branching.

As illustrated in Fig. 11, the coupling of micelles inevitably induces redistribution of PHPMA shell-chains surrounding the contact interfaces, in which the lateral repulsion of dense chains

hampers attack by another micelle.[8] In contrast, the loose-chain interfaces (normal to contact regions) are most susceptible to be attacked. On the other hand, the interfaces were stiffened by the dative bonds, which hampered further merging of contact cores. These effects induced the directional *end-to-end* binding of the micelles.[48] Topological branching stemmed from misplacement due to polydispersity of the sizes. Furthermore, dynamic nature of the imine bonds favoured the permeation of zinc ions into hydrophobic core-shell interfaces. These effects reinforced the transformation from nanorods, necklaces, nanowires and finally into mesoscopic supracolloidal networks.[10, 18]

The metallo-hybridized supracolloidal networks maintained constant after kept at room temperature for 5 months (Fig. S8). This perfect stability originated from the steric screening of the water-soluble shells, which presented further coaceration. To our awareness, it is the first time to report supracolloidal self-assembly *via* the dynamic covalent bonds and dative-bonding association. Moreover, post reactions endow these hierarchical nanostructures with not only excellent water-stability but also a huge specific surface area for the dative metal centres. Both are important in the rationale design of the metalloenzyme-inspired aqueous catalysts.[35-37] Therefore, this self-assembly provided a facile and versatile platform to produce the metallo-hybridized nanomaterials potential in enzyme-inspired aqueous catalysts.

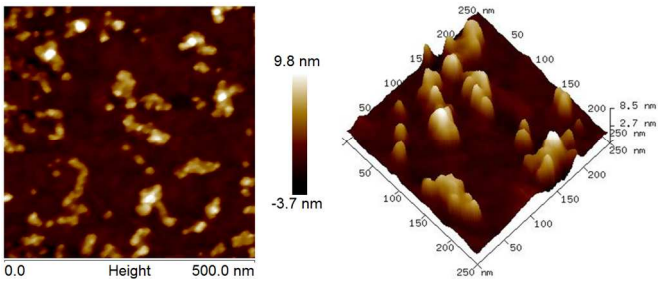

Fig. 12 AFM height and 3D images of nanostructures of $PAEMA_{57}$-*b*-$PHPMA_{56}$ formed upon the simultaneous imine conversion and coordination at a $[AEMA]_0/[PDCA]_0/[Zn(II)]_0$ = 2:1:0.3 in water at 25°C for 2 days.

Simultaneous imine conversion and metal-coordination

Since the proposal of subcomponent self-assembly by Nitschke et al.,[49] simultaneous imine conversion and coordination have been evolved as a versatile strategy to produce complex nano-materials because of effectiveness (architectures obtained via mixing simple compounds).[50-52] However, subcomponent self-assembly of the reactive polymer in water was not reported yet. Herein the approach was explored *via* starting the simultaneous reactions on alkalizing acid solution of $PAEMA_{57}$-*b*-$PHPMA_{56}$, PDCA and zinc ions to pH 9.5. UV-vis spectroscopy unveiled that the reactions were equilibrated within 6 min (Fig. S9). DLS indicated fast phase transition from water and the formation of particles with a D_h=89 nm and a μ_2/Γ^2=0.295 after the sufficient equilibration for 2 days (Fig. S10).

AFM results (Fig. 12) revealed the ill-arranged structures, in which the spherical micelles, nanorods, necklaces and irregular particles co-exist. It is not surprising because the coordination could promote not only imine conversion but also stabilization of the dynamic imine bonds,[41, 44] which hampered adjustment of the chain-conformations into a thermodynamic stable state. Moreover, spontaneous formation of hydrophobic Zn(II)-dative motifs led to immediate collapse and entanglement of polymer chains, thus the formation of irregular aggregates. These effects impeded directional assembly into well-defined nanostructures. Therefore, it is indispensable for the supracolloidal assembly to be carried out following the sequence of micellization and then coordination of the micelles in water.

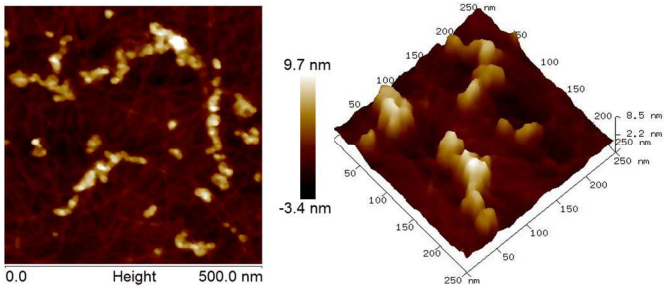

Fig. 13 AFM height and 3D images of the nanostructures of $PAEMA_{57}$-*b*-$PHPMA_{56}$ formed after the dissociation of the equilibrated nanostructures (bottom images in Fig. 9) by acidified to pH 5.5 and then assembled by alkalized again to pH 9.5.

Reversibility of metal-coordinated directional nanostructures

As-obtained solution of nanowires (see *bottom images* in Fig. 9) was used to illustrate the reversibility in assembly-disassembly of Zn(II)-coordinated nanostructures in response to solution pH. The solution was firstly acidified to pH 5.5 and then alkalized again to pH 9.5. DLS revealed the dissociation on acidifying to pH 5.5, which led to a significant decrease in light scattering intensity (2.6 kcps). ^{1}H NMR signals of AEMA units were fully detected, indicating that the imine bonds and dative bonds have been cleaved in the acidic solution. Weck and co-workers[29] also demonstrated the disassembly of chain-like colloidal structures on addition of a competitive ligand. Both the observations have demonstrated that the dative-bonding association is the driving force for the directional supracolloidal self-assembly.

Further alkalization to pH 9.5 induced the phase separation, indicated by an increase in light scattering intensity (41.7 kcps), but it was much smaller than the original (105.0 kcps). DLS analysis indicated the formation of aggregates at a D_h=105 nm with a broadened dispersity of 0.307. AFM revealed formation of irregular aggregates (Fig. 13) that are similar to those formed in a simultaneous imine conversion and coordination (Fig. 12). These results demonstrate essentially the same processes as the simultaneous reactions.

Effect of water-soluble shells on supracolloidal self-assembly

$PAEMA_{47}$-*b*-$PHPMA_{247}$ ($DP_{AEMA}/DP_{HPMA}\approx1/5$) was selected to elucidate the influence of water-soluble shells on supracolloidal assembly. UV-vis spectroscopy unveiled that the micellization and the coordination were equilibrated quickly (Fig. S11). DLS results revealed the formation of micelles at a D_h=35 nm after PDCA-conjugation (Fig. S12), but the variation in size induced by the coordination was negligible (D_h=37 nm). These results demonstrate that above-observed directional assembly has been

minimized because of the significant repulsion caused by long-chain hydrophilic $PHPMA_{247}$-shells.

Indeed, as shown in Fig. 14, the soft spherical micelles with overall sizes of 30~35 nm in diameter and 5~6 nm in height were observed after conjugation with PDCA. Moreover, these spheres virtually maintained after Zn(II)-coordination. These results demonstrate that, different from as-observed directional assembly in Fig. 10, the coordination occurred overwhelmingly within each isolated micelle owing to the significant repulsion of $PHPMA_{247}$-shells. Consequently, the PHPMA-shells played important roles not only in the above-observed stabilization of hierarchical structures but also in the directional self-assembly of these block-copolymer micelles.

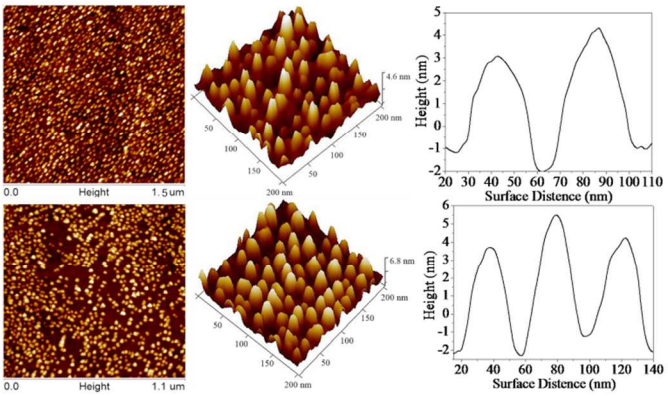

Fig. 14 AFM height and 3D images and the cross-sections (*from left to right*) of the nanostructures of PDCA-conjugated $PAEMA_{47}$-*b*-$PHPMA_{247}$ micelles (*top*) and those after the coordination at $[Zn(II)]_0/[ligand]_0$=0.3 (*bottom*) in water.

Conclusions

This article described a versatile platform for directional supra-colloidal self-assembly *via* dynamic covalent bonds and dative bonding with abundant first-row transition metal ions in water. PAEMA-*b*-PHPMA block copolymers were synthesized. Their micellization was achieved by the conjugation with PDCA via dynamic imine bonds. Dative-bonding association was used to mediate the reconstruction of these micelles. Reversible imine conversion, dehydration and micellization, and sequentially reconstruction by virtue of the coordination with copper ions and zinc ions were studied using ^{1}H NMR, UV-vis and FTIR spectroscopy, DLS, AFM and TEM.

These results have demonstrated the formation of spherical micelles after conversion into hydrophobic ligand motifs. The reversible imine bonds facilitate permeation of metal ions into hydrophobic core-shell interfaces, and coordination promotes full conversion into the imine bonds. Coordination has exerted opposite controls over the reconstruction of micelles, in which Cu(II)-coordination occurs overwhelmingly within each micelle but Zn(II)-coordination leads to directional stepwise assembly of these micelles. Thus it induces reconstruction from nanorods, nanowires, necklaces and eventually to the hierarchical supra-colloidal networks up-scaling to several tens of micrometres. The water-soluble shells play important roles in the directional assembly and stabilization of nanostructures. The post reactions of the imine conversion and Zn(II)-coordination on their core-shell interfaces endows the supracolloidal networks with a huge specific surface area for the hydrophobic dative metal centres. The pH-responsive assembly-disassembly of these micelles can be achieved by the formation-cleavage of dynamic imine bonds. In contrast, Zn(II)-coordinated nanostructures are irreversible in response to the solution pH owing to immediate collapse and entanglement of polymer chains during the simultaneous imine conversion and coordination. Hence, this directional assembly provided a general and versatile platform to produce metallo-hybridized hierarchical nanomaterials that are promising in the metalloenzyme-inspired aqueous catalysts.[34-37]

Acknowledgements

This research work was supported by National Natural Science Foundation of China (21274097, 21474069, 21334004) and the Priority Academic Program Development of Jiangsu Higher Education Institutions.

Notes and references

The Suzhou Key Laboratory of Macromolecular Design and Precision Synthesis, Department of Polymer Science and Engineering, College of Chemistry, Chemical Engineering and Materials Science, Soochow University, Suzhou 215123, P. R. China. E-mail: ylcai@suda.edu.cn; Tel & Fax: +86-512-65884419

1. S. Dutta, A. Bhaumik and K. C. W. Wu, *Energy Environ. Sci.*, 2014, **7**, 3574-3592.
2. E. K. Lim, T. Kim, S. Paik, S. Haam, Y. M. Huh and K. Lee, *Chem. Rev.*, 2015, **115**, 327-394.
3. L. Cademartiri and K. J. M. Bishop, *Nat. Mater.*, 2015, **14**, 2-9.
4. A. H. Groschel, F. H. Schacher, H. Schmalz, O. V. Borisov, E. B. Zhulina, A. Walther and A. H. E. Müller, *Nat. Commun.*, 2012, **3**, 710.
5. A. H. Groschel, A. Walther, T. I. Lobling, J. Schmelz, A. Hanisch, H. Schmalz and A. H. E. Müller, *J. Am. Chem. Soc.*, 2012, **134**, 13850-13860.
6. A. H. Groschel, A. Walther, T. I. Lobling, F. H. Schacher, H. Schmalz and A. H. E. Müller, *Nature*, 2013, **503**, 247-251.
7. W. K. Li, I. Kanyo, C. H. Kuo, S. Thanneeru and J. He, *Nanoscale*, 2015, **7**, 956-964.
8. J. H. Kim, W. J. Kwon and B. H. Sohn, *Chem. Commun.*, 2015, **51**, 3324-3327.
9. S. C. Glotzer and M. J. Solomon, *Nat. Mater.*, 2007, **6**, 557-562.
10. H. Y. Lee, S. H. R. Shin, A. M. Drews, A. M. Chirsan, S. A. Lewis and K. J. M. Bishop, *ACS Nano*, 2014, **8**, 9979-9987.
11. M. R. Jones, R. J. Macfarlane, B. Lee, J. A. Zhang, K. L. Young, A. J. Senesi and C. A. Mirkin, *Nat. Mater.*, 2010, **9**, 913-917.
12. M. R. Jones and C. A. Mirkin, *Nature*, 2012, **491**, 42-43.
13. Y. F. Wang, Y. Wang, D. R. Breed, V. N. Manoharan, L. Feng, A. D. Hollingsworth, M. Weck and D. J. Pine, *Nature*, 2012, **491**, 51-61.
14. D. Ortiz, K. L. Kohlstedt, T. D. Nguyen and S. C. Glotzer, *Soft Matter*, 2014, **10**, 3541-3552.
15. Y. Wang, Y. F. Wang, X. L. Zheng, G. R. Yi, S. Sacanna, D. J. Pine and M. Weck, *J. Am. Chem. Soc.*, 2014, **136**, 6866-6869.
16. H. Wang, L. Y. Chen, X. S. Shen, L. F. Zhu, J. T. He and H. Y. Chen, *Angew. Chem. Int. Ed.*, 2012, **51**, 8021-8025.
17. J. W. Zhou, G. R. Whittell and I. Manners, *Macromolecules*, 2014, **47**, 3529-3543.

18. X. Z. Yan, S. J. Li, T. R. Cook, X. F. Ji, Y. Yao, J. B. Pollock, Y. H. Shi, G. C. Yu, J. Y. Li, F. H. Huang and P. J. Stang, *J. Am. Chem. Soc.*, 2013, **135**, 14036-14039.
19. H. L. Li and L. X. Wu, *Soft Matter*, 2014, **10**, 9038-9053.
20. J. Y. Zhang, Y. P. Chen, K. P. Miller, M. S. Ganewatta, M. Bam, Y. Yan, M. Nagarkatti, A. W. Decho and C. B. Tang, *J. Am. Chem. Soc.*, 2014, **136**, 4873-4876.
21. M. Zhu, M. Z. Rong and M. Q. Zhang, *Polym. Int.*, 2014, **63**, 1741-1749.
22. A. C. Jackson, F. L. Beyer, S. C. Price, B. C. Rinderspacher and R. H. Lambeth, *Macromolecules*, 2013, **46**, 5416-5422.
23. D. E. Przybyla, C. M. R. Perez, J. Gleaton, V. Nandwana and J. Chmielewski, *J. Am. Chem. Soc.*, 2013, **135**, 3418-3422.
24. X. de Hatten, D. Asil, R. H. Friend and J. R. Nitschke, *J. Am. Chem. Soc.*, 2012, **134**, 19170-19178.
25. F. Freire, J. M. Seco, E. Quinoa and R. Riguera, *J. Am. Chem. Soc.*, 2012, **134**, 19374-19383.
26. P. Guillet, C. Mugemana, F. J. Stadler, U. S. Schubert, C. A. Fustin, C. Bailly and J. F. Gohy, *Soft Matter*, 2009, **5**, 3409-3411.
27. J. Brassinne, C. Mugemana, P. Guillet, O. Bertrand, D. Auhl, C. Bailly, C. A. Fustin and J. F. Gohy, *Soft Matter*, 2012, **8**, 4499-4506.
28. J. Brassinne, J. P. Bourgeois, C. A. Fustin and J. F. Gohy, *Soft Matter*, 2014, **10**, 3086-3092.
29. Y. F. Wang, A. D. Hollingsworth, S. K. Yang, S. Patel, D. J. Pine and M. Weck, *J. Am. Chem. Soc.*, 2013, **135**, 14064-14067.
30. Y. Shi, G. H. Liu, H. Gao, L. C. Lu and Y. L. Cai, *Macromolecules*, 2009, **42**, 3917-3926.
31. J. Y. Tong, Y. Shi, G. H. Liu, T. Huang, N. Xu, Z. G. Zhu and Y. L. Cai, *Macromol. Rapid Commun.*, 2013, **34**, 1827-1832.
32. G. Koz, N. Ozdemir, D. Astley, M. Dincer and S. T. Astley, *J. Mol. Struct.*, 2010, **966**, 39-47.
33. B. de Bruin, E. Bill, E. Bothe, T. Weyhermuller and K. Wieghardt, *Inorg. Chem.*, 2000, **39**, 2936-2947.
34. E. Huerta, P. J. M. Stals, E. W. Meijer and A. R. A. Palmans, *Angew. Chem. Int. Ed.*, 2013, **52**, 2906-2910.
35. D. E. Bergbreiter, *ACS Macro Lett.*, 2014, **3**, 260-265.
36. T. Terashima, T. Mes, T. F. A. De Greef, M. A. J. Gillissen, P. Besenius, A. R. A. Palmans and E. W. Meijer, *J. Am. Chem. Soc.*, 2011, **133**, 4742-4745.
37. N. Madhavan, C. W. Jones and M. Weck, *Acc. Chem. Res.*, 2008, **41**, 1153-1165.
38. Y. Shi, H. Gao, L. C. Lu and Y. L. Cai, *Chem. Commun.*, 2009, 1368-1370.
39. G. H. Liu, H. Shi, Y. R. Cui, J. Y. Tong, Y. Zhao, D. J. Wang and Y. L. Cai, *Polym. Chem.*, 2013, **4**, 1176-1182.
40. C. W. Scales, Y. A. Vasilieva, A. J. Convertine, A. B. Lowe and C. L. McCormick, *Biomacromolecules*, 2005, **6**, 1846-1850.
41. X. W. Wu, N. Xu, Z. G. Zhu, Y. L. Cai, Y. Zhao and D. J. Wang, *Polym. Chem.*, 2014, **5**, 1202-1209.
42. C. Godoy-Alcantar, A. K. Yatsimirsky and J. M. Lehn, *J. Phys. Org. Chem.*, 2005, **18**, 979-985.
43. C. B. Minkenberg, L. Florusse, R. Eelkema, G. J. M. Koper and J. H. van Esch, *J. Am. Chem. Soc.*, 2009, **131**, 11274-11275.
44. X. J. Chen, N. Xu, N. Li, L. C. Lu, Y. L. Cai, Y. Zhao and D. J. Wang, *Soft Matter*, 2013, **9**, 1885-1894.
45. J. R. Kumpfer and S. J. Rowan, *ACS Macro Lett.*, 2012, **1**, 882-887.
46. C. Bazzicalupi, A. Bianchi, C. Giorgi, P. Gratteri, P. Mariani and B. Valtancoli, *Inorg. Chem.*, 2013, **52**, 2125-2137.
47. J. Pyun, *Angew. Chem. Int. Ed.*, 2012, **51**, 12408-12409.
48. D. Kim, W. D. Kim, M. S. Kang, S.-H. Kim and D. C. Lee, *Nano Lett.*, 2015, **15**, 714-720.
49. J. R. Nitschke, *Acc. Chem. Res.*, 2007, **40**, 103-112.
50. T. K. Ronson, S. Zarra, S. P. Black and J. R. Nitschke, *Chem. Commun.*, 2013, **49**, 2476-2490.
51. I. A. Riddell, Y. R. Hristova, J. K. Clegg, C. S. Wood, B. Breiner and J. R. Nitschke, *J. Am. Chem. Soc.*, 2013, **135**, 2723-2733.
52. A. M. Castilla, W. J. Ramsay and J. R. Nitschke, *Acc. Chem. Res.*, 2014, **47**, 2063-2073.

TOC Graphic

Enzyme-inspired supracolloidal networks are now available by directional self-assembly of copolymer micelles *via* interfacial Zn(II)-coordination of dynamic covalent-bonded ligand motifs.